BOREAS An international journal of Quaternary research

Understanding processes of sediment bleaching in glacial settings using a portable OSL reader

GEORGINA E. KING, DAVID C. W. SANDERSON, RUTH A. J. ROBINSON AND ADRIAN A. FINCH

BOREAS

King, G. E., Sanderson, D. C. W., Robinson, R. A. J. & Finch, A. A. 2014 (October): Understanding processes of sediment bleaching in glacial settings using a portable OSL reader. *Boreas*, Vol. 43, pp. 955–972. 10.1111/bor.12078. ISSN 0300-9483.

Analysis of a high-resolution suite of modern glacial sediments from Jostedalen, southern Norway, using a portable optically stimulated luminescence (OSL) reader, provides insights into the processes of sediment bleaching in glacial environments at the catchment scale. High-magnitude, low-frequency processes result in the least effective sediment bleaching, whereas low-magnitude, high-frequency events provide greater bleaching opportunities. Changes in sediment bleaching can also be identified at the scale of individual bar features: tails of braid-bars and side-attached bar deposits have the lowest portable reader signal intensities, as well as the smallest conventional OSL residual doses. In addition to improving our understanding of the processes of sediment bleaching, portable reader investigations can also facilitate more rapid and comprehensive modern analogue investigations, which are commonly used to confirm that the OSL signals of modern glacial sediments are well bleached.

Georgina E. King (georgina.king@unil.ch), Department of Earth and Environmental Sciences, University of St Andrews, Irvine Building, North Street, St Andrews, Fife KY16 9AL, UK (present address: Institute of Earth Surface Dynamics, University of Lausanne, Quartier UNIL-Mouline, BâtimentGéopolis, 1015 Lausanne, Switzerland), Ruth A. J. Robinson and Adrian A. Finch, Department of Earth and Environmental Sciences, University of St Andrews, Irvine Building, North Street, St Andrews, Fife KY16 9AL, UK; David C. W. Sanderson, Department of Environmental Physics, Scottish Universities Environmental Research Centre, Rankine Avenue, Scottish Enterprise Technology Park, East Kilbride G75 OQF, UK; *received 20th October 2013, accepted 19th February 2014.*

Optically stimulated luminescence (OSL) dating, is used to successfully date Quaternary sediments in a range of different depositional environments (cf. Wintle 2008; Rhodes 2011). However, one of the key challenges to the successful application of the technique is selecting sediments that have had their luminescence signal fully reset prior to deposition. Whereas partial resetting (bleaching) is not generally expected in aeolian deposits, sediments deposited by fluvial (e.g. Murray *et al.* 1995) or glacial processes (e.g. Rhodes & Pownall 1994) can be seriously affected. One approach for assessing the degree of sediment bleaching is through the measurement of the luminescence signal of a modern analogue deposit, which has the same or a similar depositional setting to the geological deposits under investigation (Gemmell 1997; Alexanderson 2007; Bøe *et al.* 2007; Alexanderson & Murray 2012). However, recent studies into the variability of residual OSL ages in modern glacifluvial sediments has revealed that residual ages vary significantly amongst similar depositional settings, ranging from zero to almost 3000 years for glacifluvial bar deposits from a single catchment (King *et al.* 2013). Where OSL dating has been used to date glacial deposits (cf. Thrasher *et al.* 2009) a range of different residual (unbleached) luminescence signals have been reported for sediments with similar depositional settings from modern analogue investigations (e.g. Alexanderson & Murray 2012). It is therefore possible that inherited residual ages will be over- or underestimated if based on a single modern analogue deposit, which is problematic if the residual age comprises a significant proportion of the sample burial age. Considering the importance of signal resetting to successful OSL analyses, it is clear that there is further scope for detailed modern analogue studies to investigate the processes of sediment bleaching within different depositional settings.

The purpose of the present study was to investigate catchment scale variability in the residual signals of modern glacial sediments that have contrasting sediment sources and transport histories, in order that the processes of sediment bleaching may be better understood. Understanding which sediments are most likely to have experienced significant bleaching within glacial environments will inform sampling protocols and may therefore improve the accuracy and precision of OSL dating in glacial settings.

Exploring variations in luminescence signals at the catchment scale is difficult because of the significant time required to prepare OSL samples (weeks to months dependent on sample) and for their measurement (days to weeks, dependent on sample), coupled with the often challenging properties of quartz from glacial environments (e.g. Rhodes & Bailey 1997). Quartz has conventionally been regarded as the preferred mineral for OSL dating in environments where partial bleaching is likely to occur, as its most readily bleached OSL signal components can reset more rapidly than corresponding

DOI 10.1111/bor.12078

signals in feldspars, providing that the illumination field is rich in the near-UV spectrum. However, the sensitivity (brightness) of quartz from glacial sediments is often very low, which necessitates increased measurement time as many aliquots are rejected, and in the worst instances it may not be possible to obtain a quartz OSL age (e.g. Lukas *et al.* 2007).

Over the past 10 to 15 years, a number of OSL screening methods have been developed that aim to provide insights into the luminescence properties of sediments more rapidly than through conventional OSL analyses. These methods can be grouped into instrumental developments such as the Scottish Universities Environmental Research Centre portable OSL reader (Bishop *et al.* 2005; Sanderson & Murphy 2010), and methodological developments such as laboratory profiling (Sanderson *et al.* 2001, 2003; Burbidge *et al.* 2007), rangefinder ages (Durcan *et al.* 2009; Roberts *et al.* 2009) and standardized growth curves (e.g. Roberts & Duller 2004). A number of studies have recently been published that have successfully utilized one (or often more) of these techniques to characterize deposits from different environments, enabling archaeological and environmental questions to be more rapidly addressed (e.g. Muñoz-Salinas *et al.* 2012; Munyikwa *et al.* 2012). Kinnaird *et al.* (2012) used a combination of portable reader (PR) data and laboratory profiling analyses to gain insights into the palaeoenvironmental history of a coastal setting in Orkney, Scotland. Stang *et al.* (2012) also contrasted PR data with rapid profiling analyses on untreated sediments using a Risø TL/OSL reader to investigate the history of soil mixing in the San Gabriel Mountains, USA. The work reported here uses a combination of rapid portable reader measurements, and conventional OSL analyses in order to better understand the likely bleaching opportunities that different glacial and glacifluvial sediments experience throughout transport and deposition at both the catchment and individual landform scales.

Study area

The Jostedalen region of southern Norway is host to the Jostedalsbreen icecap, which is the largest body of ice in mainland Europe (Fig. 1). The Jostedal Plateau is thought to have completely deglaciated 7.5–5.5 cal. ka BP (Nesje & Kvamme 1991; Matthews *et al.* 2000; Nesje *et al.* 2000, 2001), but has experienced significant Neoglaciation since ~5 ka BP (Shakesby *et al.* 2004). Various outlet glaciers drain Jostedalsbreen and samples were collected from the Jostedøla (JOS), but four catchments are the focus areas of this research: Bergsetdalen (BERG), Fåbergstølsdalen (FAB), Fåbergstølsgrandane (GRAN) and Nigardsdalen (MJO).

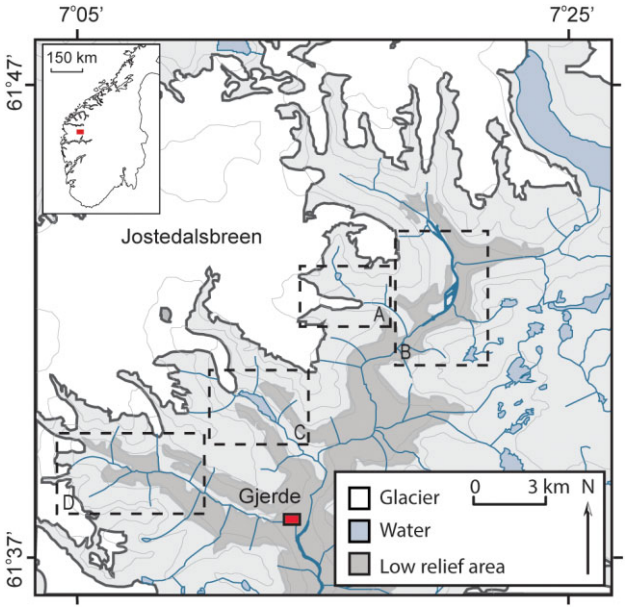

Fig. 1. Map of the Jostedalen region of southern Norway with study sites highlighted: A = Fåbergstølsdalen; B = Fåbergstølsgrandane; C = Nigardsdalen; D = Bergsetdalen. This figure is available in colour at http://www.boreas.dk.

Jostedalen is within the western Gneiss region of Norway (Bryhni & Sturt 1985), and is underlain by bedrock of Precambrian granitic to granodioritic gneiss (Holtedahl 1960; Holtedahl & Dons 1960). The upper catchments of Nigardsbreen and Bergsetdalen are underlain by quartz monzanite, whilst Fåbergstø lsdalen and the majority of Jostedalen are underlain by quartz diorite.

Fåbergstølsdalen (FAB)

Fåbergstølsbreen (61°42′N, 7°17′E) discharges into the E–SE trending Fåbergstølsdalen valley and is drained by a single meltwater stream, which anastomoses in the lower catchment. Very little vegetation is established in the upper catchment where till and early Holocene paraglacial deposits are reworked by debris flows (Ballantyne & Benn 1994), which form the dominant sediment source in addition to direct subglacial inputs. Fåbergstølsdalen has a high degree of hillslope connectivity and debris flow material is transported directly into the meltwater stream. The Fåbergstølsdalen catchment is 3 km^2 and 19 samples of glacifluvial bars were collected along a transect of 2.5 km from the ice front, as well as five samples from paraglacial, subglacial and avalanche deposits, which represent sediment sources.

Bergsetdalen (BERG)

Bergsetbreen (61°38′51N, 7°06′16E) is a hanging glacier that discharges into the E–NE orientated Krundalen valley, the upper section of which is referred

to as Bergsetdalen. It is the most southern valley sampled within Jostedalen, and is heavily vegetated relative to Fåbergstølsdalen. Sediments are sourced predominantly from subglacial material, although limited reworking of paraglacial deposits within the Little Ice Age (LIA) moraine limit (Bickerton & Matthews 1993) also contributes to the total sediment budget of this catchment. Material is transported by the meltwater stream, which is a similar size to the meltwater stream in Fåbergstølsdalen, but comprises multiple braided bars in the upper catchment and a single meltwater channel in the lower catchment. The Bergsetdalen catchment is 7 km^2, and 27 samples were taken predominantly from braided bars in the upper catchment, but also from side-attached bar deposits 3 km from the ice front. Bergsetdalen forms a complementary sample site to Fåbergstølsdalen, as meltwater streams form a significant mode of transport in both catchments but Bergsetdalen does not have the high degree of channel-hillslope connectivity of Fåbergstølsdalen. Contrasting these sites may enable the influences of depositional processes and sediment sources to be separated and identified.

Fåbergstølsgrandane (GRAN)

Fåbergstølsgrandane (61°43′39N, 7°21′50E) is the largest sandur in mainland Norway and occupies a catchment of 6 km^2. It is sourced from a number of the Jostedalsbreen outlet glaciers including the debris-covered Lodalsbreen within Stordalen. Sediment sources are dominantly subglacial, although paraglacial material from Stordalen and Trongedalen will also contribute to the total sediment flux, in addition to material avalanched directly onto the sandur from the valley sides. The Jostedøla river is sourced from these catchments and flows across the western and southern flanks of the sandur, and is bordered by a suite of side-attached bar deposits. Fåbergstølsgrandane comprises a series of braided bars, which range from heights of 1 m above the channel bottom in the upper northwest part of the sandur, which is most proximal to the source sediments, to heights of ~30 cm further east and southeast. Clast sizes vary as bar heights reduce from cobble-dominated bars in the northwest to gravel- and sand-dominated bars in the southeast. Samples were collected across two transects. The first comprised nine samples of braided bar deposits and was 1.5 km in length, and the second comprised 11 samples of side-attached bar deposits and was 2 km in length.

Nigardsdalen (MJO)

Subglacial sediment from Nigardsbreen forms the dominant sediment source in Nigardsdalen. Sediment is transported by the meltwater stream into a proglacial lake where a fan delta composed of braided bar deposits is formed. The bars have maximum heights of 30 cm across the delta, and clast sizes range from gravels to sands, although occasional cobbles are found in the most glacier-proximal bars. Nigardsdalen forms a complementary site to Fåbergstølsgrandane, as although the scale of the braid-bars is smaller, they are formed from similar depositional processes. The Nigardsdalen proglacial delta has shallower relief than the Fåbergstølsgrandane sandur, and the braid-bars will be submerged more regularly in response to small changes in meltwater discharge. It is difficult to provide an estimate of the delta size because the exposed area varies depending upon lake level; however, it ranges from approximately 0.03 to 0.08 km^2. Fifteen braid-bar deposits were sampled, as well as a single sample of paraglacial sediment near to the ice front.

Sample collection

The objective of this research was to explore the luminescence signals of modern sediments, rather than explore the relative chronologies of different deposits. Sample modernity was ensured through sampling horizons that are >2 cm but within a few cm of the sediment surface. Samples from all sites with the exception of Nigardsdalen were collected through covering the sample site with an opaque, plastic bag and sampling directly into transparent sample bags within opaque plastic bags. Samples from Nigardsdalen were collected in opaque plastic tubes. Mainly glacifluvial deposits were sampled as glacifluvial transport and depositional processes are dominant in all of the catchments with the exception of Fåbergstølsdalen, where debris flows contribute significantly to the total sediment flux. Additional samples of subglacial, paraglacial and supraglacial material were taken to characterize other key sediment sources and transport and depositional processes within glacial environments.

Portable reader analyses

Portable reader analyses were carried out using the 2005 Scottish Universities Environmental Research Centre (SUERC) prototype reader in the laboratories at SUERC. Whereas conventional OSL methods are usually applied to a restricted grain size and a single mineral (except polymineral fine-grained analyses), the portable reader facilitates simple measurements of the luminescence response of the multi-mineral bulk deposit without pre-treatment. Under subdued light conditions, 96 bulk samples were decanted into 50 mm Petri dishes for PR analysis and were not given any pre-treatment.

Full details of the SUERC-PR are given in Sanderson & Murphy (2010). The system comprises IR (880 nm) and blue (470 nm) diodes, and luminescence

Table 1. A. Portable reader analysis protocol. Stimulation sources are indicated in parentheses. PSP = post-stimulation phosphorescence. B. Feldspar analysis protocol.

A	
Background 1	10 s (no stimulation)
IRSL	80 s (IR diode stimulation)
IRSL PSP	10 s (no stimulation)
Background 2	10 s (no stimulation)
BSL	80 s (blue diode stimulation)
BSL PSP	10 s (no stimulation)
B	
Natural/regenerative doses	6.2, 12.4, 18.6, 0, 6.2 Gy[1]
TL	250°C, 60 s, 5°C s^{-1}
IRSL	50°C, 100 s, 5°C s^{-1}, 90% power
Test dose	6.2 Gy
TL	250°C, 60 s, 5°C s^{-1}
IRSL	50°C, 100 s, 5°C s^{-1}, 90% power
IRSL	290°C, 100 s, 5°C s^{-1}, 90% power

[1]Regenerative doses varied dependent upon sample *De* but initial analyses were carried out with these doses. IRSL = infra-red stimulated luminescence, PSP = post-stimulation phosphorescence, BSL = blue stimulated luminescence, TL = thermoluminescence.

is detected through UG11 filters using an ETL photodetector module with a 25 mm bi-alkali photomultiplier. The prototype system was capable of continuous-wave stimulation and detection only, and was reliant on manual operation of the stimulation diodes.

The sample measurement sequence used here had 200 s duration comprising a 10 s background acquisition (i.e. no diode stimulation), followed by 80 s IR stimulated luminescence (IRSL) measurement and a subsequent 10 s post-stimulation phosphorescence (PSP) plus background measurement (i.e. no diode stimulation, Sanderson & Murphy 2010). The IRSL measurements were immediately followed by blue stimulated luminescence (BSL) measurements in the same format and for the same duration (Table 1A). All measurements were performed at room temperature, and samples were not dried prior to analysis. Samples were stored for between one and four weeks at room temperature before measurement.

The luminescence signals measured from multi-mineral bulk sediments are the product of numerous variables, which have been discussed by Sanderson & Murphy (2010). They are dependent on (i) the postdepositional age of the sediment, (ii) the total radiation dose that the sediment has been exposed to during burial, (iii) the degree of signal resetting through sunlight exposure that the sediment experienced prior to deposition, (iv) the sensitivity (brightness) of the luminescence signal of the minerals present, and (v) the sediment grain-size. This research aims to isolate only one of these controls on the luminescence signals, namely point (iii), which relates to the unbleached fraction of the initial luminescence signal and is referred to as the residual luminescence.

The residual signal of a sediment is the product of the initial luminescence signal of its constituent minerals, and the degree of sunlight exposure that it has experienced throughout transport and deposition. Through sampling only modern material, the influence of the postdepositional age of the sediment (point (i)) has been circumvented. The influence of the total radiation dose that the samples have received, point (ii), is complex as a residual dose can relate to the dose rate of the sediment source location, rather than the sample location. However, as measured dose rate variations within the different catchments are small (RSD <16%; King 2012), these will have less influence on the resultant luminescence signals than the effects of partial bleaching. Sample luminescence will also be affected by changing concentrations of different minerals (point (iv)) with different luminescence sensitivities, and by changing grain size populations which experience different bleaching opportunities (point (v)); however, such variations may also encode information about the depositional and transport processes that the sediment has experienced.

OSL sample preparation for conventional analyses

Four K-feldspar samples (JOS13, JOS14, JOS18 and JOS51) were prepared specifically for comparison with the portable reader analyses using conventional methods. Material was desiccated at 50°C to enable calculation of water content, and sieved to extract the 180–212 μm grain size fraction selected for analysis. The 180–212 μm grain-size fraction was treated with 30% HCl to remove $CaCO_3$ and with H_2O_2 to remove organics. K-feldspar was extracted from the polymineral sample through density separations and the <2.58 g cm^{-3} K-feldspar fraction was not etched (Duller 1992).

Conventional OSL analyses

All conventional OSL analyses were carried out at the University of St Andrews using either a TL-DA-15 (Bøtter-Jensen *et al.* 2003) or TL-DA-20 Risø reader, equipped with an EMI 9235QA photomultiplier. The detection region was restricted to the blue for the K-feldspar samples using a Corning 7–59 and BG-39 filter. Infrared (~870 nm) diodes were used for stimulation and a $^{90}Sr/^{90}Y$ beta source was used for irradiations. Equivalent dose values were calculated using Analyst v.3.22b (Duller 2005).

Feldspar OSL was measured using small (2 mm, ~30 grain) multi-grain aliquots, and a modified single

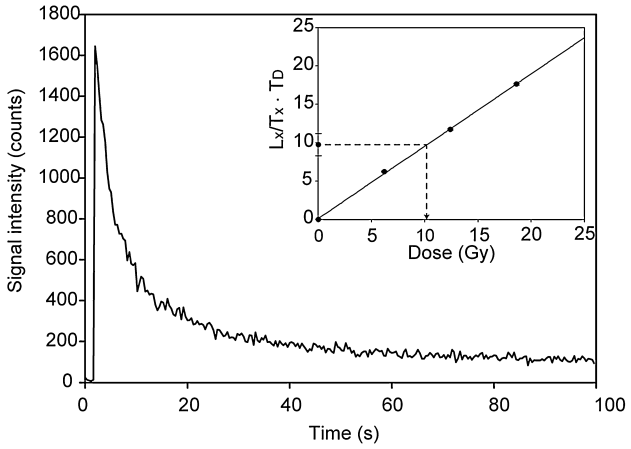

Fig. 2. Typical K-feldspar conventional IRSL decay curve measured using a Risø TL/OSL laboratory system. The inset shows the standardized growth curve for sample JOS13. The standardized growth curve was constructed from the average dose response of 12 aliquots (1σ uncertainties are within the data points). The average $L_n/T_n \bullet T_D$ value for all 48 aliquots of JOS13 is shown on the *y*-axis with 1 standard error uncertainties.

aliquot regenerative (SAR) dose protocol (Wallinga *et al.* 2000) whereby the first and second preheat temperatures are identical in order to improve sensitivity corrections (after Huot & Lamothe 2003; Blair *et al.* 2005; Wallinga *et al.* 2007; Table 1B). A high-temperature IR bleach was incorporated at the end of each SAR cycle (Murray & Wintle 2003; Blair *et al.* 2005; Buylaert *et al.* 2007), which is designed to deplete excess signal that may accumulate throughout analysis (recuperation). The recently developed post-IR IRSL protocol (Thomsen *et al.* 2008; Buylaert *et al.* 2009), which is less susceptible to anomalous fading (Wintle 1973), was not employed as it is not suitable for young sediments or those that may be partially bleached (Thiel 2011).

The suitability of the selected protocol (Table 1B) was confirmed through a range of dose-recovery and preheat-plateau experiments. Acceptance criteria are (i) recycling ratios within 10% of unity, (ii) signal intensities ≥3σ above background, (iii) recuperation within 10% of the normalized maximum regenerated dose, and (iv) D_e value uncertainties are ≤10%. K-feldspar D_e values were not corrected for anomalous fading, as contrasts in relative residual ages rather than the absolute residual ages are of key interest.

Standardized growth curves (SGC) for quartz and polymineral fine grains have recently been investigated by a number of authors (e.g. Roberts & Duller 2004). A set of individual SGCs for each of the four samples were developed from which D_e values could be interpolated (Fig. 2). Standardized growth curve development greatly increased the rate of analysis. The suitability of the calculated SGCs was evaluated through comparing D_e values calculated from interpolation of the sensitivity-corrected natural luminescence signal (L_n/T_n) onto the SGC with those obtained from a full SAR protocol fitted in Analyst v.3.22b (Duller 2005). To avoid circularity, aliquots used for testing the SGCs were not included in their construction. Fitting uncertainty was calculated using LINEST in Excel 2007, and incorporated together with 1.5% analytical uncertainty.

Dose rate calculations

The environmental radiation dose rate (D_r) must be determined in order to calculate sample residual age. It is comprised of external contributions from cosmic radiation and the decay of radio-isotopes in the sedimentary matrix, as well as from internal contributions from the decay of radio-isotopes within the minerals themselves. The concentrations of U, Th, K and Rb were measured directly using ICP-MS at the University of St Andrews. It was not possible to calculate D_r for JOS13 and instead the average value for JOS14 and JOS18 has been used. The K-feldspar samples analysed were not etched, and therefore an alpha contribution to their D_r has also been incorporated. Alpha and beta attenuation factors after Bell (1980), Mejdahl (1979) and Readhead (2002a, b) were used and conversion factors after Adamiec & Aitken (1998). A concentration of 12% K was assumed for the internal β-dose of K-feldspar samples (Huntley & Baril 1997), and an a-value of 0.15±0.05 (Balescu & Lamothe 1992). Following calculation of D_r (Gy ka^{-1}), sample age was calculated: Age (ka) = D_e/D_r (Table 2).

Table 2. Age-modelled D_e values and calculated ages. All samples were modelled with the three-component minimum age model (Galbraith & Laslett 1993), which was selected using the criteria of Bailey & Arnold (2006) with revised critical values (Arnold 2006) after Thrasher *et al.* (2009).

Sample	n	D_e (Gy)	Water content (%)	K (%)	Th (ppm)	U (ppm)	Rb (ppm)	Dry Alpha dose rate (Gy ka^{-1})	Wet Dose rate (Gy ka^{-1})	Age (ka)
JOS13	48	3.63±0.43	14.8	3.05±0.18	12.21±0.71	2.52±0.15	124.30±6.21	0.30±0.35	4.26±0.33	0.85±0.12
JOS14	45	2.52±0.27	18.5	2.82±0.16	12.77±0.75	2.99±0.17	115.40±5.78	0.33±0.35	4.28±0.33	0.59±0.08
JOS18	47	2.76±0.21	21.7	3.28±0.19	11.65±0.68	2.04±0.12	133.20±6.66	0.27±0.35	4.36±0.34	0.63±0.07
JOS51	47	2.78±0.16	25.3	3.55±0.21	14.86±0.87	3.66±0.21	100.00±5.00	0.40±0.36	5.00±0.36	0.56±0.05

Results and discussion

Portable reader analyses

Net IRSL, BSL, IRSL/BSL ratios and PSP were calculated following signal background corrections for all measurements (Table 3). Signals were background corrected using the preceding dark count measurement to avoid PSP. All samples exhibited measurable luminescence signals that exceeded system dark counts (Fig. 3). Luminescence decay curves are similar for the BSL and IRSL signals, and both can be well fitted with an exponential decay (r^2>0.9, Fig. 3). All of the samples exhibited brighter BSL than IRSL, and samples with dim IRSL also had dim BSL. Stimulating a deposit with infra-red light, prior to blue light can help to isolate the luminescence contributions of different minerals (e.g. Roberts 2007). However, quartz emissions are much less bright than feldspar emissions, and it is thus likely that both IRSL and BSL signals measured from these bulk samples at room temperature are predominantly from feldspars. This is supported by the strong correlation (r^2 = 0.93) between BSL and IRSL signal intensities for all samples (Fig. 4A).

Post-stimulation phosphorescence was brightest following BSL, and there is a positive correlation between BSL and background-corrected BSL PSP (r^2 = 0.60), and IRSL and background-corrected IRSL PSP (r^2 = 0.47; Fig. 4B). The subtle variations in PSP intensity, beyond that explained by differences in IRSL and BSL signal intensities, may reflect variations in mineral composition between samples (Sanderson & Murphy 2010). This paper is concerned with exploring catchment scale changes in sample luminescence residual signals and therefore no further investigations into the causes of PSP variability have been carried out at this stage.

Contrasting portable reader and conventional OSL analyses of glacial sediments

Prior to investigating the application of portable reader luminescence measurements to explore the unbleached residual luminescence signals of glacial sediments, it is necessary to understand what the different luminescence signals are responding to. A suite of 27 glacial sediment samples from Jostedalen, which have been previously investigated using conventional quartz and K-feldspar OSL SAR analyses (King *et al.* 2013; 2014), and four K-feldspar samples described here, were also analysed using the portable reader. Portable reader net signal intensities, IR/BSL ratios and conventional OSL age-modelled ages, overdispersion values and average test dose signal intensities (T_x, Table 3) were contrasted using Pearson's correlation coefficient (Table 4), calculated in RStudio (R Development Core Team 2011). The test dose is fixed within SAR protocols in order to monitor sensitivity changes, identified as changing luminescence responses, throughout analysis (Murray & Wintle 2000) and provides information regarding the luminescence sensitivity (brightness) of a sample.

Net signal intensities. – For the majority of samples, there is no correlation between the portable reader net signal intensities and T_x signal intensity. However, whereas the coarse-grained K-feldspar T_x signal intensities of samples from Fåbergstølsgrandane exhibit no relationship with the portable reader signal (r = 0.310). Coarse-grained quartz T_x signal intensities of the same samples do correlate with the portable reader net IRSL signals (r = 0.648), and portable reader net BSL signals (r = 0.697), although neither of these correlations is significant at the 95% confidence interval. In contrast the coarse-grained K-feldspar T_x signal intensities of samples from Nigardsdalen are well correlated with the portable reader net IRSL signal (r = 0.930), which is significant at the 95% confidence interval, and with the portable reader net BSL signals (r = 0.739). On this basis therefore, portable reader net signal intensities may be considered indicative of the sensitivity of the coarse-grained quartz and/or K-feldspar extracts for some, but not all, of the samples presented here.

The portable reader net signal intensities were also contrasted with the age-modelled conventional OSL ages for the different deposits, and all samples exhibit a positive correlation of r≥0.576. Where the quartz and K-feldspar samples are grouped together and analysed, statistically significant correlations are recorded between net IRSL and net BSL and the age-modelled ages for both minerals. Portable reader results are therefore informative about the age-modelled ages of different glacial sediments, which is commonly the most important output of conventional OSL dating.

IR/BSL ratios. – Conventional OSL analyses from these catchments have revealed these deposits to be partially bleached with wide and variable D_e distributions (e.g. King *et al.* 2013), as measured using the sample overdispersion values (σ_d). The variability in the degree of signal resetting is clearly visible in the portable reader data, which vary in intensity over several orders of magnitude. Some studies have reported differential bleaching between quartz and feldspar in glacifluvial depositional settings (e.g. Klasen *et al.* 2007: fig. 6); therefore, the relative net intensities of the IRSL and BSL signals may also encode information about the degree of partial bleaching of sediments. However, this can only be determined through calculating the IR/BSL ratios of a range of deposits because a baseline IR/BSL ratio must be established. This is because different luminescence signals have different signal intensities, and thus the BSL signal may be brighter than the IRSL signal, whilst relating to a dose of equal amount.

Overdispersion values range from zero to 84±13% across the sample suite (Table 3), but the same degree

Table 3. SUERC-PR and conventional OSL data summary. m = distance from ice margin. Samples without an overdispersion (σ_d) value have fewer than 20 aliquots.

Sample		Type	m	Net IRSL	Net BSL	IR/BSL	IRSL PSP	BSL PSP	Quartz age (ka)	Quartz (σ_d)	K-feldspar age (ka)	K-feldspar (σ_d)
BERG	11	Braid bar	412	47 183	153 741	0.307	478	1681				
	12	Braid-bar-mid	480	124 790	359 684	0.347	1160	2741				
	20	Side-attached bar	3064	2749	15 814	0.174	111	175				
	21	Braid-bar-mid	201	137 807	449 540	0.307	1124	3053				
	22	Braid-bar-mid	203	151 854	454 775	0.334	1286	1788				
	23	Braid-bar-head	315	84 246	275 926	0.305	824	2060				
	24	Braid-bar-head	318	50 062	157 732	0.317	609	923				
	25	Braid-bar-mid	320	2006	12 614	0.159	100	271				
	26	Braid-bar-mid	555	69 469	214 961	0.323	586	1694				
	27	Braid-bar-mid	384	163 598	512 356	0.319	1090	5054				
	28	Braid-bar-mid	314	101 188	327 764	0.309	918	3019				
	29	Braid-bar-mid	380	162 422	529 568	0.307	1375	4456				
	30	Braid-bar-mid	1445	7553	36 865	0.205	173	496				
	31	Braid-bar-tail	1408	19 280	78 348	0.246	287	1761				
	32	Side-attached bar	1443	4344	23 806	0.182	131	406				
	34	Braid-bar-mid	1416	39 010	151 781	0.257	365	1502				
	35	Braid-bar-tail	575	75 852	268 707	0.282	697	1456				
	36	Braid-bar-mid	515	56 184	199 718	0.281	–	–				
	37	Braid-bar-mid	453	41 027	184 123	0.223	–	–				
	38	Braid-bar-mid	468	29 883	109 639	0.273	350	988				
	39	Braid-bar-mid	469	7622	32 866	0.232	121	533				
	40	Braid-bar-mid	470	22 553	99 588	0.226	345	1018				
	64	Braid-bar-mid	0	103 550	340 867	0.305	–	–				
	65	Braid-bar-mid	0	100 486	329 585	0.304	–	–				
	66	Braid-bar-mid	0	28 998	122 463	0.237	–	–				
	88	Supraglacial	0	1058	6423	0.165	–	–				
	89	Moraine	248	96 751	292 119	0.331	–	–				
FAB	2	Subglacial	0	71 845	235 489	0.305	703	2226	1.72±0.77	0.68±0.10		
	41	Paraglacial	109	343 346	840 582	0.408	1129	4746	3.31±0.24	–		
	42	Avalanche	109	11 064	52 264	0.212	165	435	0.20±0.07	0.91±0.11		
	78	Side-attached bar	0	47 387	162 361	0.292	506	1827				
	79	Side-attached bar	0	254 448	646 139	0.380	2315	3958	4.06±1.04	0.47±0.05		
	80	Side-attached bar	99	201 777	580 825	0.347	1647	2590	1.64±0.45	–		
	81	Side-attached bar	146	102 119	374 511	0.273	928	3044				
	82	Side-attached bar	248	54 645	159 248	0.342	506	1223				
	83	Side-attached bar	341	199 257	565 115	0.353	1640	4601				
	84	Side-attached bar	386	295 075	801 908	0.367	1915	5432	1.13±0.34	0.84±0.13		
	85	Paraglacial	577	47 103	143 239	0.328	391	1062	0.39±0.16	0.87±0.12		
	86	Paraglacial	669	199 734	589 146	0.339	1933	3412	0.89±0.63	0.91±0.12		
	87	Side-attached bar	894	169 109	527 614	0.321	–	–				
	90	Side-attached bar	889	169 218	498 056	0.339	1450	1566	2.82±1.08	–		
	91	Side-attached bar	889	228 801	630 233	0.363	1994	4365	1.34±0.28	0.67±0.07		
	92	Side-attached bar	909	9500	61 532	0.154	163	703	0.00±0.10	0		
	93	Side-attached bar	943	167 003	481 536	0.347	1907	3229				
	94	Side-attached bar	986	92 752	255 660	0.363	–	–	1.64±0.42	0.64±0.06		
	95	Side-attached bar	1026	58 213	171 131	0.340	–	–	2.36±0.63	0.61±0.05		
	96	Side-attached bar	980	22 306	85 539	0.261	–	–				
	97	Side-attached bar	1070	212 593	595 887	0.321	–	–				
	99	Side-attached bar	1242	124 663	401 436	0.311	848	2932	1.50±0.54	0.50±0.07		
	100	Side-attached bar	1494	80 956	319 944	0.253	806	1707	0.65±0.29	0.83±0.11		
	101	Side-attached bar	2056	289 378	792 699	0.365	1944	4581				
GRAN	1	Side-attached bar	3225	82 186	272 685	0.301	8355	0				
	2	Side-attached bar	3335	66 549	232 418	0.286	439	1341				
	76	Side-attached bar	4313	3743	22 391	0.167	124	266				
	77	Side-attached bar	4304	15 464	53 262	0.290	167	568				
	54	Braid-bar-head	825	219 002	695 090	0.315	1920	2090	5.39±0.55	–	33.6±3.49	0.20±0.01
	55	Braid-bar-mid	771	150 577	511 821	0.294	1117	2594	3.29±0.21	0.27±0.01	22.8±2.53	0.25±0.01
	56	Braid-bar-tail	934	33 649	123 489	0.271	282	872	0.47±0.07	0	2.77±0.32	0.24±0.01
	57	Braid-bar-tail	1184	16 379	73 671	0.222	181	716	0.94±0.10	0	1.98±0.24	0.35±0.02
	58	Braid-bar-head	1344	195 689	599 791	0.326	2084	3672	3.38±1.03	0.24±0.01	26.6±8.36	0.24±0.00
	60	Braid-bar-mid	1569	24 836	75 981	0.321	182	734				
	61	Braid-bar-mid	1847	156 030	484 085	0.322	1100	3651				
	62	Braid-bar-mid	2104	106 610	380 062	0.281	714	2386				
	63	Braid-bar-mid	1715	379 137	958 522	0.397	1633	5485				
	69	Side-attached bar	2079	22 402	103 868	0.216	2366	946			1.18±0.13	0.61±0.04
	70	Side-attached bar	2204	24 995	121 998	0.204	242	1127				

Table 3. Continued

Sample		Type	m	Net IRSL	Net BSL	IR/BSL	IRSL PSP	BSL PSP	Quartz age (ka)	Quartz (σ_d)	K-feldspar age (ka)	K-feldspar (σ_d)
	71	Side-attached bar	2378	5940	21 235	0.280	99	241				
	72	Side-attached bar	2890	12 211	29 452	0.205	177	554				
	73	Side-attached bar	3119	46 035	163 790	0.281	330	1974				
	74	Side-attached bar	3102	14 506	58 919	0.246	194	431				
	75	Side-attached bar	3206	26 156	106 940	0.245	191	567				
JOS	51	Side-attached bar	>10 km	7251	28 142	0.258	829	288			0.56±0.05	0.27±0.02
	52	Side-attached bar	>10 km	2807	20 300	0.138	108	233				
	53	Side-attached bar	>10 km	2576	15 084	0.171	104	236				
	13	Braid-bar-head	>10 km	14 113	48 256	0.292	153	223			0.85±0.12	0.67±0.06
	14	Braid-bar-mid	>10 km	8164	31 958	0.255	130	170			0.59±0.08	0.74±0.07
	15	Braid-bar-mid	>10 km	7319	25 825	0.283	147	301				
	16	Braid-bar-mid	>10 km	8506	28 086	0.302	122	367				
	17	Braid-bar-head	>10 km	14 102	48 345	0.292	249	801				
	18	Braid-bar-tail	>10 km	3695	15 988	0.231	65	216			0.63±0.07	0.46±0.03
MJO	3	Braid-bar-tail	477	8627	40 950	0.211	169	325			1.45±0.24	0.34±0.02
	4	Braid-bar-mid	455	644 586	1 389 662	0.464	2314	3191			19.0±3.02	0.54±0.03
	5	Braid-bar-head	432	70 274	207 580	0.339	420	680				
	6	Braid-bar-head	412	262 752	1 286 351	0.204	727	2499			3.18±0.31	0.61±0.04
	7	Braid-bar-mid	536	47 276	136 478	0.346	129	378			0.91±0.10	0.31±0.02
	8	Braid-bar-tail	544	15 729	67 291	0.234	107	283			1.24±0.14	0.22±0.01
	9	Braid-bar-head	528	60 761	166 185	0.369	437	513			0.96±0.11	0.75±0.07
	10	Braid-bar-head	262	325 414	660 559	0.493	1230	1721				
	44	Braid-bar-mid[1]	444	456 116	1 277 255	0.357	610	6985				
	45	Braid-bar-mid[1]	508	65 506	169 830	0.386	447	424				
	45a	Braid-bar-mid[1]	497	9804	47 423	0.207	154	550				
	46	Braid-bar-mid	472	85 488	256 785	0.333	570	1310				
	47	Braid-bar-mid[1]	508	360 829	936 704	0.385	2044	5718				
	48	Braid-bar-tail	558	82 864	252 510	0.328	732	1325				
	49	Braid-bar-head	477	40 773	146 714	0.279	319	1029				
	50	Paraglacial	0	84 839	257 336	0.330	489	2159				

[1]Manual operation error resulted in no PSP measurement.

of variability is not recorded within the IR/BSL ratios: values range from 0.14 to 0.50. Changing IR/BSL ratios are likely to be dependent upon the influx of sediments of unsorted mineralogy, as well as variable sunlight exposure histories, whereas the over-dispersion values of conventional single-aliquot OSL measurements reflect the differential bleaching of minerals of a single type (assuming that there are no mineral inclusions) and grain size. Correlation coefficients are also low between IR/BSL ratios and overdispersion values (Table 4), which highlights that for these samples portable reader IR/BSL ratios are relatively insensitive to the effects of partial bleaching, in comparison to conventional single-aliquot OSL analyses. This may be a consequence of measuring the luminescence response of grams, rather than milligrams of material as is done in conventional single-aliquot OSL investigations, or alternatively reflect that a different variable, such as mineralogical composition is controlling the changing IR/BSL ratios of these deposits. It is also likely that both the IR and post-IR BSL signals are dominated by the luminescence response of feldspars, masking any differential bleaching between quartz and feldspar.

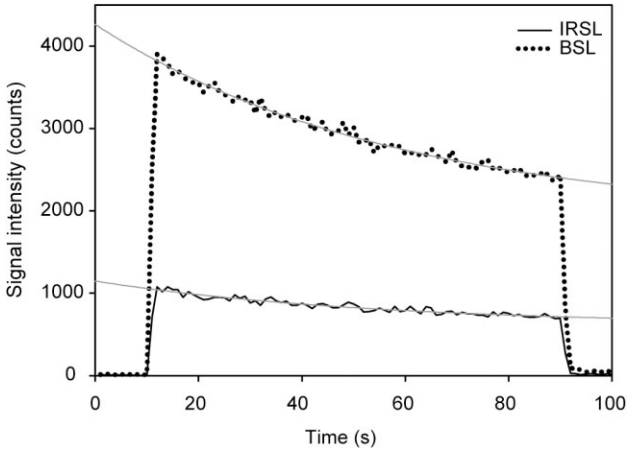

Fig. 3. IRSL and BSL decay curves measured using the SUERC portable reader system for side-attached bar sample GRAN62; both signals fitted with an exponential decay.

Summary of comparisons between portable reader and conventional SAR analyses. – Comparison of the portable reader and conventional SAR data for a range of different glacial sediments has shown that the portable reader analyses provide an effective screening mecha-

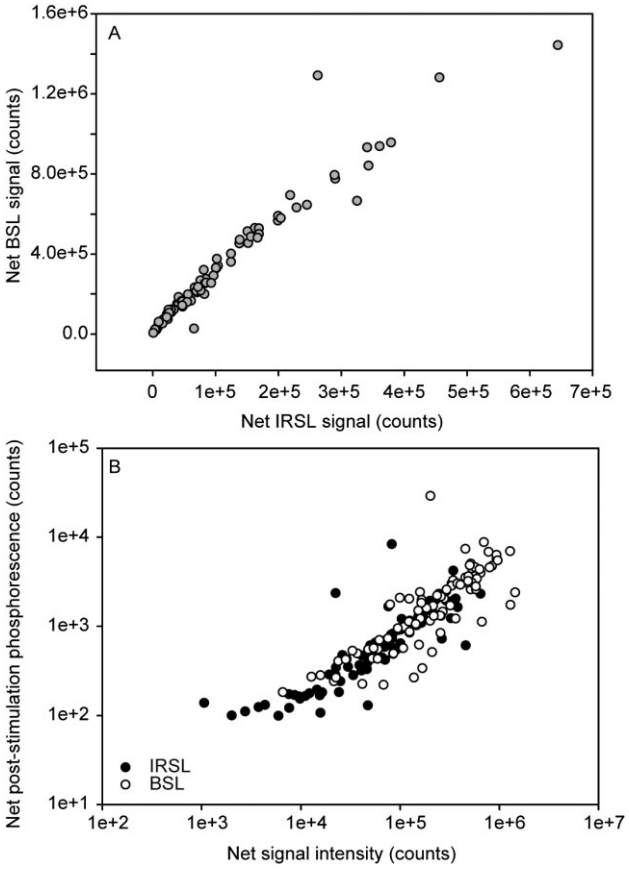

Fig. 4. A. Correlation of net IRSL and BSL signal intensities. B. Correlation of net signal intensities and poststimulation phosphorescence for all samples analysed.

nism for relative OSL sample age using either the IRSL or BSL net signal intensities. However changing IR/BSL ratios are unable to identify heterogeneous bleaching in individual samples, which is the key cause of overdispersion measured during conventional OSL analyses for these different glacial deposits. Instead the ratios most likely reflect changing mineralogical compositions of the deposits, either by provenance or as a function of sediment sorting throughout transport and deposition. These comparisons show that portable reader analyses provide useful insights into the conventional OSL properties of individual mineral and grain-size extracts, and their relative residual doses. The remainder of this paper will explore the potential of portable reader analyses for the investigation of sediment bleaching within glacial environments.

Portable reader analyses of sediments from the Jostedøla

The majority of samples analysed in this research are modern glacifluvial deposits that comprise either side-attached or braid-bars which are proximal to the ice front (within 3 km). Within glacial environments, partial bleaching of sediments that have been transported over relatively short distances is known to be problematic (e.g. Berger 1990). A suite of six braid-bar deposits and three side-attached bar deposits were analysed from the Jostedøla river at distances >10 km from any glacial source. As these sediments have been transported much greater distances than the sediments analysed from the glacial catchments, they are more likely to have had their luminescence signals fully reset and provide a control on the effects of partial bleaching, which are often attributed to short transport distances within glacial environments.

The IRSL and BSL signal intensities vary between the different side-attached bar and braid-bar deposits, and braid-bar-head deposits have the greatest IRSL and BSL signal intensities. The average IRSL signal intensity for the braid-bar head deposits is 14 108±8 counts (n = 2, uncertainty is the standard deviation at 1σ), and the average BSL signal intensity is 48 837±21 counts. In contrast, the braid-bar-mid deposits sampled have average IRSL signal intensity of 7996±611 counts and average BSL signal intensity of 29 120±3304 counts

Table 4. Pearson's r correlation coefficients for conventional SAR OSL analyses and portable reader net IRSL, BSL and IRSL/BSL ratios. Ages are the age-modelled ages, maximum ages are calculated from the highest D_e value measured for a single aliquot of each sample. σ_d = overdispersion.

Mineral	Site	n	Pearson's r					
			Net IRSL vs. average T_x signal intensity	Net BSL vs. average T_x signal intensity	Net IRSL vs. age	Net BSL vs. age	n	IR/BSL vs. σ_d
Quartz	FAB	15	0.259	0.184	0.629	0.576	13	–0.194
Quartz	GRAN	5	0.648	0.697	0.748	0.817	–[2]	–
Feldspar	GRAN	6	0.310	0.254	0.842[1]	0.928[1]	6	–0.226
Feldspar	MJO	6	0.930[1]	0.739	0.966[1]	0.765	6	0.361
Feldspar	JOS	4	0.069	0.048	0.795	0.752	4	0.384
Quartz		20	0.287	0.224	0.654[1]	0.657[1]	18	0.186
Feldspar		16	0.315	0.294	0.625[1]	0.607[1]	16	0.096

[1]Significant at the 95% confidence interval.

[2]Not calculated as the majority of samples have zero overdispersion.

(n = 3), i.e. braid-bar-mid deposits have signals ~50% smaller than braid-bar-head deposits. The braid-bar-tail deposit (JOS18) has the lowest IRSL (3695 counts) and BSL (15 988 counts) signal intensities of the braid-bar deposits. Following the good correlation between portable reader signal intensities and SAR quartz and K-feldspar age-modelled ages, the different signal intensities between the bar-heads, bar-mids and bar-tail are interpreted to reflect improved sediment bleaching and reducing residual doses with transport across the bar features, rather than changing mineralogical compositions. This may be a consequence of changing water depths, and increased opportunities for subaerial exposure during transport across braid-bars.

The side-attached bar deposits have similar luminescence properties to the braid-bar-mid and -tail deposits; IRSL signal intensities are 4211±2643 counts and BSL signal intensities are 20 277±4891 counts (n = 3). This suggests that side-attached bar deposits are also better bleached than braid-bar-head deposits, and that the braid-bar-mid and tail deposits and side-attached bar deposits have experienced similar degrees of sediment bleaching, perhaps due to having similar exposure potential as a consequence of similar transport processes and rates. Whereas braid-bar-head deposits are essentially comprised of higher grain sizes and sediment that accumulates under deeper and more turbulent flows, sediment on braid-bar-mids, -tails and side-attached bars may be transported under lower energy conditions and at lower transport rates across the bar, providing improved bleaching opportunities.

The coarse-grain (180–212 μm) K-feldspar fraction of a braid-bar-head (JOS13), -mid (JOS14) and -tail deposit (JOS18), as well as one of the side-attached bar deposits (JOS51), have been dated using a SAR protocol, resulting in ages of <1 ka (Table 2). The braid-bar-head deposit (JOS13) has the greatest residual age (0.85±0.12 ka) of the deposits analysed, whereas the side-attached bar deposit (JOS51) has the lowest residual age (0.56±0.05 ka), which is within uncertainties of the braid-bar-mid (JOS14) and -tail (JOS18) deposits (Table 2). Overdispersion values are more variable and range from 27±2% (n = 47) for the side-attached bar deposit (JOS51), to 74±7% (n = 45) for the braid-bar-mid deposit (JOS14). An increase in overdispersion is recorded between the braid-bar-head (JOS13) and the -mid and -tail deposits (JOS14, JOS18), and is interpreted to reflect increased sediment bleaching with transport across bar features (King *et al*. 2013). The conventional OSL data support the observations made from the portable reader signal intensities, and show that sediments may not be completely bleached even after transport over >10 km from glacial source regions, but that side-attached bar deposits and braid-bar-tail deposits have both the lowest conventional OSL residual doses and portable reader luminescence signal intensities.

Portable reader analyses: Fåbergstølsdalen and Bergsetdalen

Fåbergstølsdalen. – Glacifluvial side-attached bar deposits were sampled along a transect from the ice margin up to 2 km from the glacial snout in Fåbergstølsdalen, and various source sediments including subglacial and paraglacial material were also sampled. The portable reader IRSL signal intensities of the side-attached bar deposits range from 9500 to 343 346 counts and net BSL signal intensities also vary over an order of magnitude from 52 338 to 841 870 counts. The different side-attached bar deposits sampled do not exhibit any systematic variation in IRSL net signal intensities throughout the catchment (Fig. 5), similar to the results of conventional quartz OSL analyses (Fig. 6A), which showed only a slight reduction in residual age with transport distance (King *et al*. 2013). However there is a slight reduction in BSL signal intensity with transport distance (Fig. 6B). Comparison of the portable reader IRSL and BSL net signal intensities with conventional quartz OSL data (Fig. 6) shows that they follow broadly similar trends to the age-modelled ages. Overdispersion values are more variable than the IR/BSL ratios (Fig. 6C), in agreement with the low correlation coefficient between these variables (Table 4).

The different source sediments have different luminescence signal intensities, which are dependent upon the specific deposit type. FAB42 is an avalanche deposit, and has one of the lowest IRSL signal intensities (11 064 counts) and the lowest BSL signal intensity recorded for the Fåbergstølsdalen samples. These low values can be explained by the high bleaching opportunities of material exposed at the surface following transport via avalanching, and similarly low values are obtained when this deposit is dated using conventional quartz SAR: 0.18±0.06 ka (King *et al*. 2013). In contrast, FAB41 is a slope failure deposit and has the brightest IRSL and BSL signal intensities of the Fåbergstølsdalen samples as well as one of the greatest residual ages of sediments from this catchment: 3.31±0.24 ka (King *et al*. 2013). In contrast to an avalanche deposit (e.g. FAB42), material transported by slope failure through debris flows and sheet wash (e.g. FAB41, FAB86) has more limited sunlight exposure opportunities, although this is dependent upon the scale and duration of the event. The variability in the properties of the different source sediment types highlights the variety and complexity of the different depositional processes operating within Fåbergstølsdalen.

Bergsetdalen. – Samples from Bergsetdalen were taken over a similar length transect to Fåbergstølsdalen, and the braid-bars in the ice-proximal environment <500 m from the snout were sampled most intensively. Con-

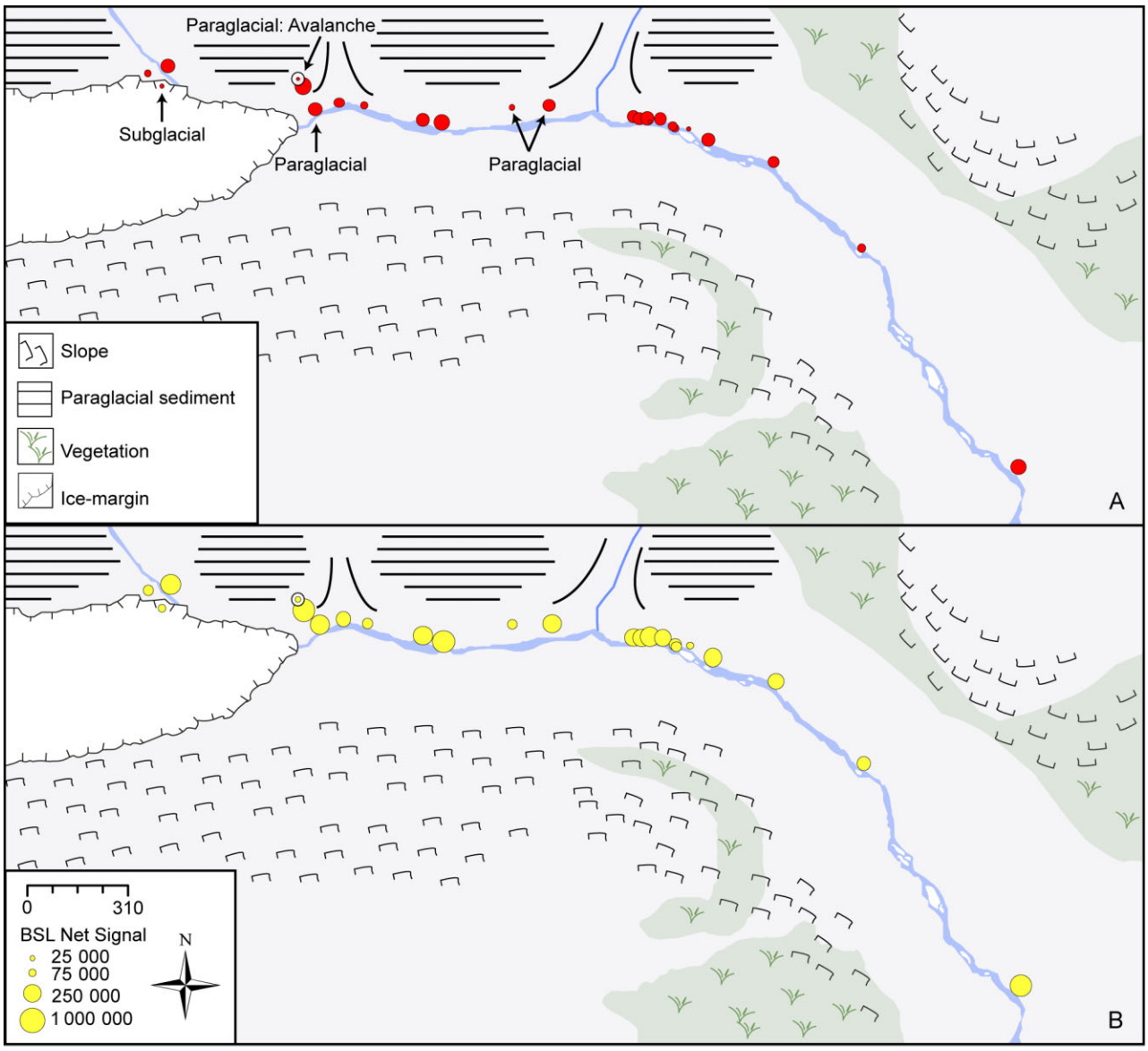

Fig. 5. Fåbergstølsdalen sample IRSL (A) and BSL (B) portable reader signals. All samples are side-attached bar deposits with the exception of those labelled as subglacial or paraglacial. This figure is available in colour at http://www.boreas.dk.

ventional quartz SAR analyses were attempted on 10 samples from Bergsetdalen; however, low signal intensities and poor recycling ratios meant that analyses were not pursued (King 2012). Samples from Bergsetdalen have amongst the lowest IRSL and BSL signal intensities of the entire sample suite (Fig. 7). IRSL and BSL signal intensities vary by one order of magnitude between the various braid-bar deposits analysed, and IRSL signals are an order of magnitude smaller than BSL signals. Two side-attached bar deposits (BERG20 and BERG32) were also sampled from Bergsetdalen, and have some of the lowest net luminescence signals recorded within the catchment (Table 3). A single supraglacial sample (BERG88) was analysed and has the lowest net BSL signal (6423 counts) and IRSL signal (1058 counts) intensities measured for the Bergsetdalen samples. This deposit is likely to be completely bleached based upon its depositional context, and thus this provides a benchmark against which the degree of bleaching of the other sediments within this catchment can be evaluated. A moraine deposit (BERG89) was also analysed from Bergsetdalen, and has a net IRSL signal intensity of 96 751 counts, which is one of the highest signal intensities measured for this catchment, although BERG27 and BERG29, which are braid-bar deposits, have the brightest net IRSL and net BSL signals, respectively.

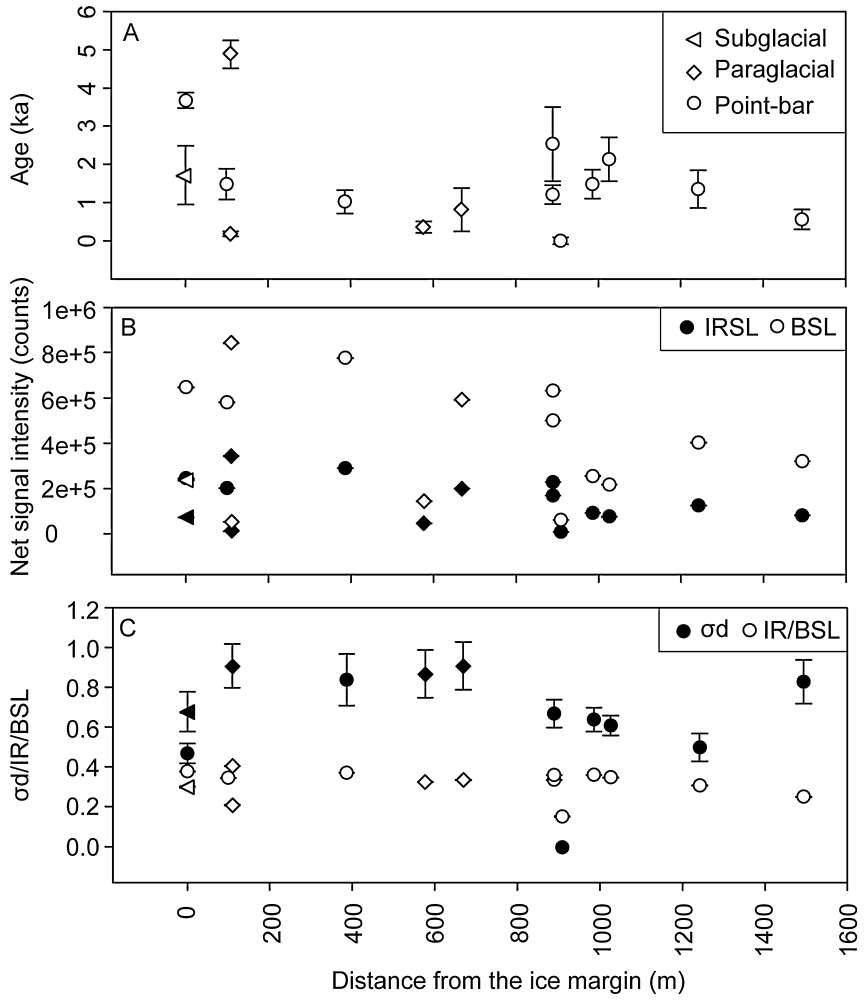

Fig. 6. Comparison of portable reader and conventional SAR data for Fåbergstølsdalen (King *et al.* 2013) plotted relative to transport distance from the ice margin. A. Conventional OSL age. B. Portable reader IRSL and BSL signal intensities. C. Overdispersion and portable reader IR/BSL ratios.

Sediments in Bergsetdalen are sourced from subglacial material and paraglacial material on the west valley side, which has been exposed by recent glacial retreat, as well as a limited volume of supraglacial material. The meltwater stream dissects a single moraine in the upper catchment, and a limited amount of material is obtained from snow avalanching; however, apart from these minor contributors there are no other direct sediment inputs into the meltwater channel. Consequently the residual luminescence signals are anticipated to reduce with transport throughout the catchment, as material has greater opportunity for sunlight exposure. A weak trend towards reducing net signal intensity with increasing transport distance was recorded in Bergsetdalen (Figs 7, 8), showing that sediments in Bergsetdalen are better bleached as meltwater transport distance increases in agreement with previous observations elsewhere (e.g. Gemmell 1999).

Comparisons of portable reader analyses: Fåbergstølsdalen and Bergsetdalen. – The residual IRSL and BSL signals in Fåbergstølsdalen were greater than those recorded in Bergsetdalen for transport over similar distances (Figs 6, 8). A slight reduction in signal with increasing transport is recorded for the BSL signal in Fåbergstølsdalen (Fig. 6B), whereas both the IRSL and BSL signals decrease in Bergsetdalen (Fig. 8). The difference in signal intensities and changing residual luminescence signals can be explained by the contrasting geomorphology and transport processes of the two catchments. Transport and deposition in Fåbergstølsdalen involve the remobilization of paraglacial sediments by debris flows throughout the entire upper catchment, whereas most of the sediment transported in Bergsetdalen is entrained from deposits within ~300 m of the glacial snout. Thus, source sediments are transported over longer distances prior to deposition in the Bergsetdalen meltwater stream, which affords improved bleaching opportunities.

If the entrainment of source materials does explain the differences in luminescence signal intensities recorded between the two catchments, then the upper 300 m of Bergsetdalen may reflect a similar variability in luminescence intensities to that recorded across the entire

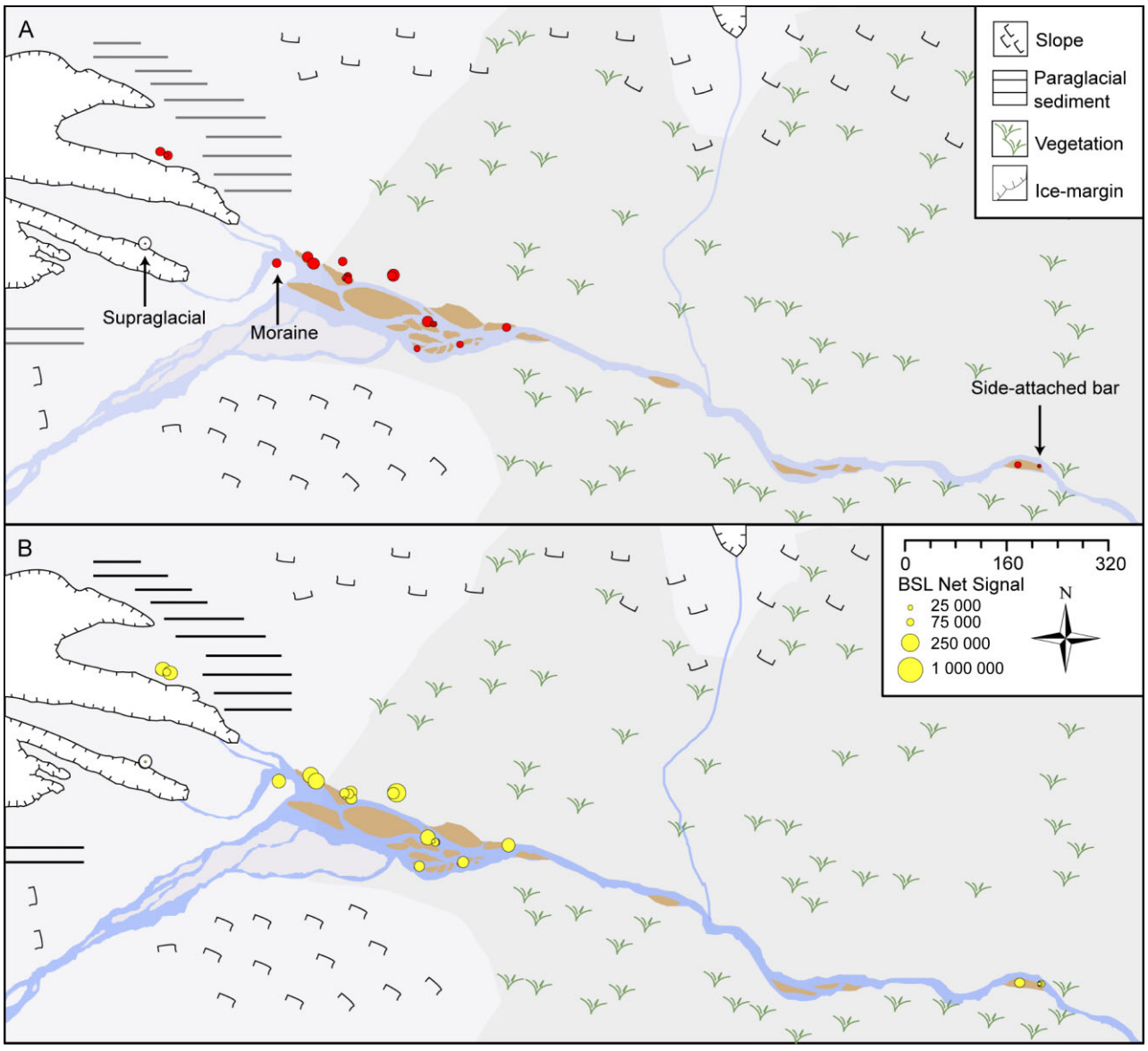

Fig. 7. Bergsetdalen sample IRSL (A) and BSL (B) portable reader signals. All samples are braid-bar deposits with the exception of those labelled as supraglacial (BERG88), moraine (BERG89) and side-attached bar (BERG32) deposits. BERG20 (side-attached bar deposit), which was sampled 3064 m from the glacial snout, is not shown. This figure is available in colour at http://www.boreas.dk.

Fåbergstølsdalen catchment. Examination of Fig. 8 shows that signals vary most in the upper catchment of Bergsetdalen, and that the range of luminescence intensities recorded for the different signals reduces with increasing transport distance; variations in signal intensities are greater than those recorded in Fåbergstølsdalen (Fig. 6B). The source sediments between the two catchments are similar, in that they comprise subglacial and paraglacial sediments; however, the total flux of paraglacial sediments in Fåbergstølsdalen is much greater. Thus, the increased variability in signal intensities recorded in Bergsetdalen is likely to reflect sediments approaching complete signal bleaching, whereas deposits in Fåbergstølsdalen retain a greater residual dose. The contrasting behaviour between Bergsetdalen and Fåbergstølsdalen shows that portable reader measurements of bulk sediments are sensitive to differences in residual luminescence signals caused by changing source sediment inputs and sediment transport processes.

Portable reader analyses: Fåbergstølsgrandane

Fåbergstølsgrandane has some of the largest and smallest residual IRSL and BSL signals of the different catchments analysed (maximum IRSL: 379 137 and maximum BSL: 958 522 counts; minimum IRSL: 3743 and minimum BSL: 21 235 counts). When considering

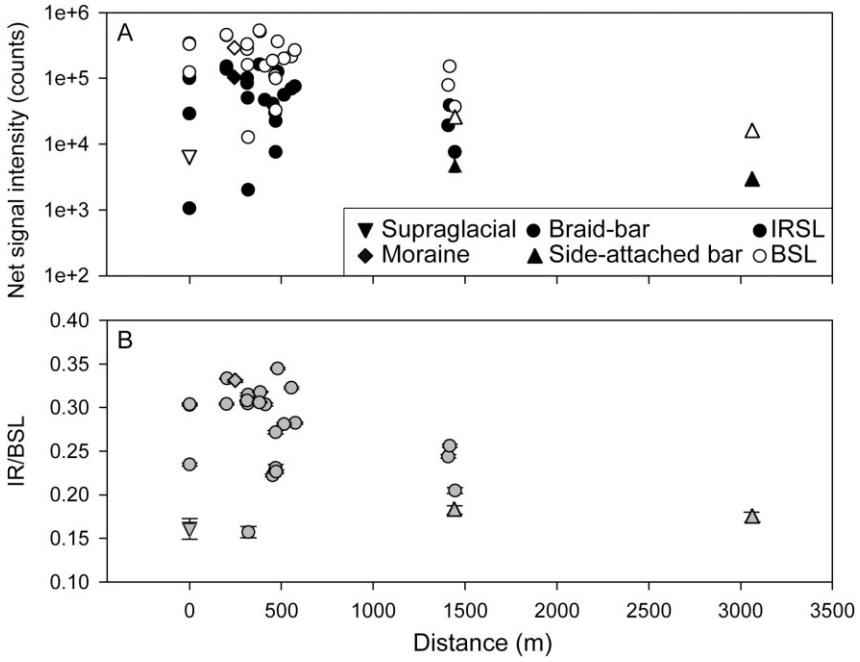

Fig. 8. Changing IRSL and BSL signal intensities (A), and IR/BSL ratios (B) with transport distance for samples from Bergsetdalen.

the spatial distribution of these data and their specific depositional contexts, the extreme values are the product of two distinct depositional environments (Fig. 9). The greatest IRSL and BSL signals are associated with braid-bar deposits along the northeast sandur side, whereas the smallest signals are associated with a suite of side-attached bar deposits adjacent to the main meltwater channel. These results are similar to those observed for braid-bar-head deposits, and braid-bar-mid, -tail and side-attached bar deposits from the Jostedøla.

The depositional setting may explain some of the contrasting luminescence properties. The various braid-bar deposits that exhibit the greatest luminescence signals are farthest from the main meltwater channel (~200 m), and thus are only mobilized during high-frequency, low-magnitude events. Turbulent flows result in limited bleaching opportunities as sunlight exposure is reduced both by attenuation of incident rays throughout a turbulent water column (Jerlov 1976) and also by rapid sediment transport. Such episodic transport of material limits the bleaching opportunities of sediments deposited at the braid-bar-heads (e.g. GRAN54, GRAN58). However, transport and quiescence across the bar features during waning flow, which results in the downstream accretion of bar tails (e.g. GRAN56, GRAN57), allows relatively more opportunities for sediment bleaching. Portable reader luminescence signals can be seen to reduce across individual bar features (Fig. 9): GRAN54, GRAN55 and GRAN56 are sampled from the braid-bar-head, -mid and -tail of the same feature. The rate of down-bar bleaching can be much higher than an average downstream bleaching rate for channel deposits, a phenomenon that is similar to the very different rates of grain-size decrease on individual bars and channel deposits (Rice & Church 2010). King *et al.* (2014) recorded the same relationship in conventional OSL dating of coarse-grained quartz and K-feldspar. Braid-bar-tail deposits therefore show the best bleached material using conventional OSL dating and also the smallest portable reader luminescence signal intensities. In contrast to the braid-bar-head deposits, the side-attached bar deposits (e.g. GRAN76), which form the second depositional environment, are reworked during moderate discharge. This results in more frequent transport events as moderate discharges occur more frequently than elevated discharges, therefore increasing the opportunities for sediment bleaching. These observations are also supported by the portable reader and K-feldspar SAR data for the side-attached bar and braid-bar deposits from the Jostedøla discussed above. There are no samples that investigate the rate of bleaching across an individual side-attached bar.

It is not possible to separate the two different depositional sub-environments for Fåbergstølsgrandane completely using the PR luminescence signals alone, because the braid-bar-tail deposits from the first environment have residual luminescence signals as low as the side-attached bar deposits. Luminescence signal intensity data cannot therefore be taken in isolation of depositional context (i.e. spatial location) when making inferences about specific depositional pathways, although it does encode information about depositional processes. Both the braid-bar-tail and

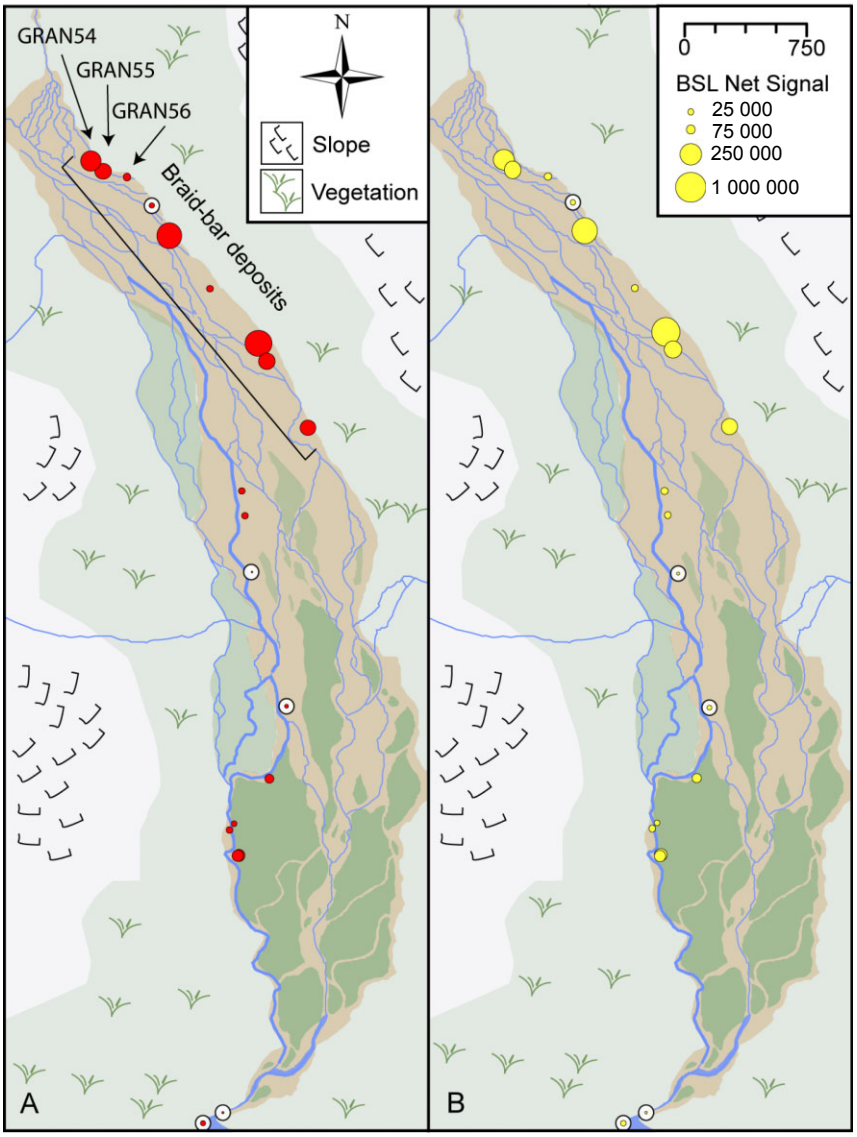

Fig. 9. Fåbergstølsgrandane sample portable reader IRSL (A) and BSL (B) signals. Braid-bar deposits are indicated, all other samples are side-attached bar deposits. This figure is available in colour at http://www.boreas.dk.

side-attached bar deposits have the lowest IRSL and BSL signals (Table 3) and are likely to be suitable for conventional luminescence dating because they are well bleached. This proposition is validated through the observations of King *et al.* (2014) that braid-bar-tail deposits have the lowest residual luminescence signals during conventional coarse-grained K-feldspar and quartz single aliquot SAR analyses; thus these data also show that the portable reader can be used as an effective screening mechanism in sample selection.

Portable reader analyses: Nigardsdalen

The final catchment investigated is Nigardsdalen, which has a dominant sediment source of subglacial material that is transported via the meltwater stream onto the proglacial fan delta. The fan delta comprises a suite of braid-bar deposits, and as such forms a similar depositional environment to that identified for the northeast of Fåbergstølsgrandane, although sediments have a maximum transport distance of ~500 m. Nigardsdalen exhibits the greatest residual luminescence intensities of the different catchments analysed (maximum IRSL: 644 586 counts, maximum BSL: 138 9662 counts; Fig. 10); however, the residual ages of bar-head deposits (e.g. MJO6) from this catchment determined from the SAR of coarse-grained K-feldspar are lower than those recorded in Fåbergstølsgrandane (King *et al.* 2014). Thus, the high residual luminescence signals are potentially caused by different mineralogy, which has greater luminescence sensitivity due to differences in the bedrock geology between the two catchments: Fåbergstølsgrandane is underlain by quartz diorite, whereas the upper catchment of Nigardsdalen is underlain by quartz monzanite. Therefore although

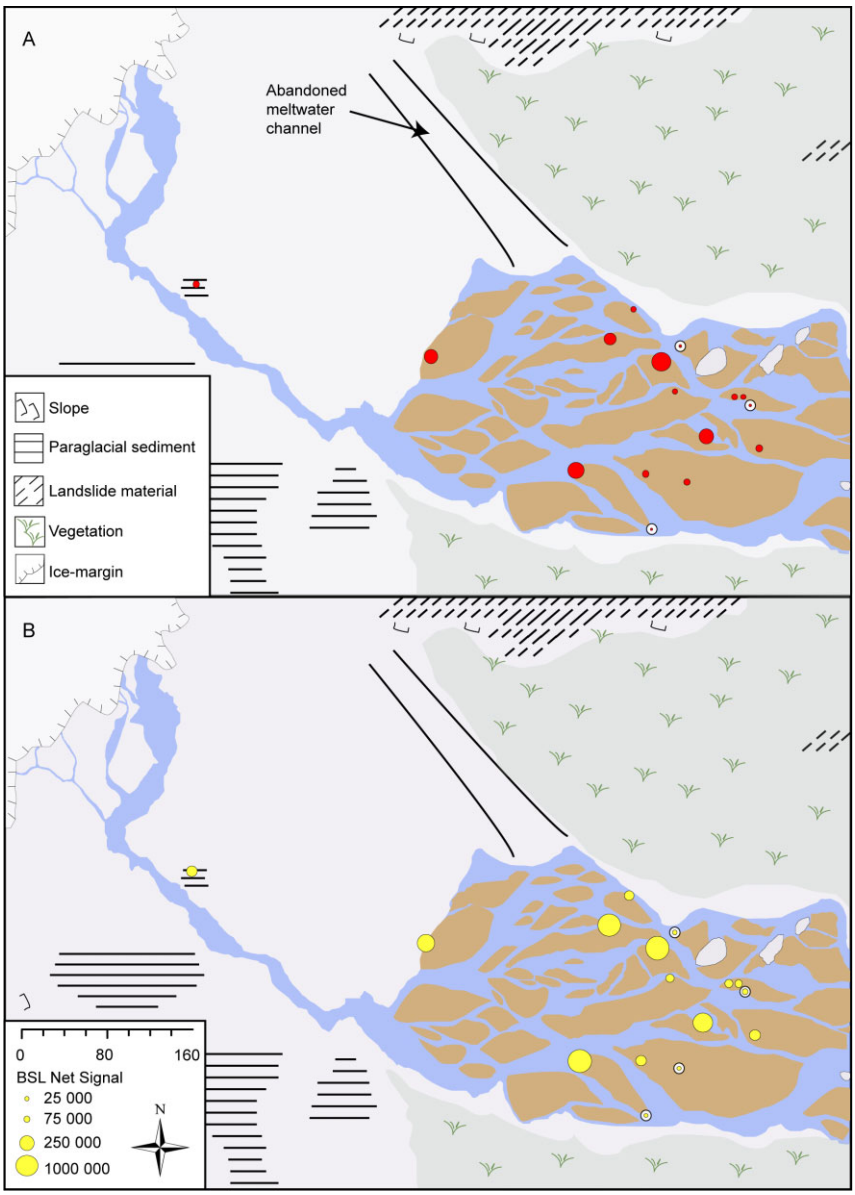

Fig. 10. Nigardsdalen sample IRSL (A) and BSL (B) portable reader signals. The single paraglacial sample is indicated (MJO50), all other samples are braid-bar deposits. This figure is available in colour at http://www.boreas.dk.

the relative signal intensities of different samples can be usefully contrasted, caution should be taken in making inferences about residual doses between catchments from signal intensity data alone.

The net IRSL and BSL signals both vary over two orders of magnitude within Nigardsdalen, and exhibit a clear reduction in signal intensity during downstream transport across the delta (Fig. 10), which is conducive with increasing opportunities for bleaching with transport distance. Improved bleaching is also visible across individual bar features, e.g. MJO9, MJO7 and MJO8 are sampled from the braid-bar-head, -mid and -tail of the same feature. A more complicated pattern is recorded amongst MJO5, MJO4 and MJO3, which are sampled from a braid-bar-head, -mid and -tail of the same feature, as MJO4 has the brightest signal intensity (IRSL 644 586 counts, BSL 138 9662 counts). This reflects the location of sample MJO4 adjacent to a cross-over chute channel, and highlights the sensitivity of luminescence signals to transport and depositional processes. Bar morphology and bar-channel interaction influence the PR luminescence signal of a sediment and again highlight the importance of careful sample selection when glacifluvial sediments are collected.

The IRSL and BSL signal intensities reduce dramatically across the fan delta, showing that bleaching occurs very rapidly over short distances (<560 m) within this depositional environment. Following from the observations discussed for braid-bar deposits from the Jostedøla and Fåbergstølsgrandane, this suggests that transport across the Nigardsdalen delta comprises multiple steps during moderate flows, rather than rapid

transport during periods of elevated discharge. This is because lower energy transport processes within this specific depositional environment results in better opportunities for sunlight exposure and sediment bleaching. The best-bleached samples are braid-bar-tail deposits (e.g. MJO3), which supports observations from the Jostedøla and Fåbergstølsgrandane that the best-bleached material in braid-bar systems is that sampled from braid-bar-tails. However, a fan delta deposit results from flow expansion and this lateral spreading (rather than vertical accumulation) of sediment may provide bleaching opportunities for more sediment grains during deposition.

Conclusions

The residual luminescence signals of different modern glacifluvial sediments sampled from a suite of different glacial catchments have been shown to vary dependent upon specific depositional setting. Use of a portable OSL reader facilitated the rapid analysis of 96 samples enabling investigation of sediment bleaching at both the catchment scale, and across individual glaciofluvial bar features. Contrasting net IRSL and BSL signals measured using the PR with conventional OSL ages has shown that for these deposits, the luminescence signals of bulk, multi-mineral samples that have experienced no pretreatment prior to measurement provide insights into conventional single mineral, single grain-size OSL ages. Residual luminescence signals reduce with increasing transport distance and associated improved bleaching opportunities in all catchments with the exception of Fåbergstølsdalen, where the influx of paraglacial material results in elevated residual luminescence signals. Braid-bar-tail deposits and side-attached bar deposits have been shown to be best bleached in a range of different glacifluvial environments. These observations will help to inform sampling procedures for conventional OSL dating applications, helping to reduce the likelihood of sampling partially reset sediments.

Modern analogue investigations are frequently employed within conventional OSL dating projects to identify depositional sub-environments which contain sediments that have been fully reset. The portable reader provides a rapid, cheap and effective means of screening samples for conventional luminescence analyses, and can be used independently with information about depositional setting to make inferences about the relative bleaching opportunities offered by different transport and depositional processes.

Acknowledgements. – G.E. King undertook this research whilst in receipt of NERC studentship F008589/1 and is SAGES affiliated. L. Carmichael and S. Fisk (SUERC) and R. Sommerville, A. Calder and D. Herd (University of St Andrews) are thanked for laboratory assistance. D. Lowry (University of St Andrews), E. Harris (Swansea University), L. Baek Nielson, C. Caballero and A. Cullens (IceTroll) are thanked for fieldwork assistance. Financial support in the form of a New Workers Research Award is acknowledged from the Quaternary Research Association. Mark Bateman and Sébastien Huot are thanked for their constructive comments on an earlier version of this manuscript.

References

Adamiec, G. & Aitken, M. J. 1998: Dose-rate conversion factors: update. *Ancient TL 16*, 37–46.

Alexanderson, H. 2007: Residual OSL signals from modern Greenlandic river sediments. *Geochronometria 26*, 1–9.

Alexanderson, H. & Murray, A. S. 2012: Luminescence signals from modern sediments in a glaciated bay, NW Svalbard. *Quaternary Geochronology 10*, 250–256.

Arnold, L. J. 2006: *Optical dating and computer modelling of arroyo epicycles in the American Southwest*. D.Phil. thesis, University of Oxford, 735 pp.

Bailey, R. M. & Arnold, L. J. 2006: Statistical modelling of single grain quartz d-e distributions and an assessment of procedures for estimating burial dose. *Quaternary Science Reviews 25*, 2475–2502.

Balescu, S. & Lamothe, M. 1992: The blue emission of K-feldspar coarse grains and its potential for overcoming TL age underestimation. *Quaternary Science Reviews 11*, 45–51.

Ballantyne, C. K. & Benn, D. I. 1994: Paraglacial slope adjustment and resedimentation following recent glacier retreat, Fåbergstølsdalen, Norway. *Arctic and Alpine Research 26*, 255–269.

Bell, W. T. 1980: Alpha dose attenuation in quartz grains for thermoluminescence dating. *Ancient TL 12*, 4–8.

Berger, G. W. 1990: Effectiveness of natural zeroing of the thermoluminescence in sediments. *Journal of Geophysical Research 95*, 12375–12397.

Bickerton, R. W. & Matthews, J. A. 1993: Little ice age variations of outlet glaciers from the Jostedalsbreen ice-cap, Southern Norway: a regional lichenometric-dating study of ice-marginal moraine sequences and their climatic significance. *Journal of Quaternary Science 8*, 45–66.

Bishop, P., Sanderson, D., Hansom, J. I. M. & Chaimanee, N. 2005: Age-dating of tsunami deposits: lessons from the 26 December 2004 tsunami in Thailand. *Geographical Journal 171*, 379–384.

Blair, M. W., Yukihara, E. G. & McKeever, S. W. S. 2005: Experiences with single-aliquot OSL procedures using coarse-grain feldspars. *Radiation Measurements 39*, 361–374.

Bøe, A. G., Murray, A. & Dahl, S. O. 2007: Resetting of sediments mobilised by the LGM ice-sheet in southern Norway. *Quaternary Geochronology 2*, 222–228.

Bøtter-Jensen, L., McKeever, S. W. S. & Wintle, A. G. 2003: *Optically Stimulated Luminescence Dosimetry*. 355 pp. Elsevier Science, Amsterdam.

Bryhni, I. & Sturt, B. A. 1985: Caledonides of southwestern Norway. *In* Gee, D. E. & Sturt, B. A. (eds.): *The Caledonide Orogen*, 89–109. John Wiley & Sons, Chichester.

Burbidge, C. I., Sanderson, D. C. W., Housley, R. A. & Allsworth Jones, P. 2007: Survey of Palaeolithic sites by luminescence profiling, a case study from Eastern Europe. *Quaternary Geochronology 2*, 296–302.

Buylaert, J. P., Murray, A. S., Thomsen, K. J. & Jain, M. 2009: Testing the potential of an elevated temperature IRSL signal from K-feldspar. *Radiation Measurements 44*, 560–565.

Buylaert, J. P., Vandenberghe, D., Murray, A. S., Huot, S., De Corte, F. & Van den Haute, P. 2007: Luminescence dating of old (>70 ka) Chinese loess: a comparison of single-aliquot OSL and IRSL techniques. *Quaternary Geochronology 2*, 9–14.

Duller, G. A. T. 1992: *Luminescence chronology of raised marine terraces, south-west North Island, New Zealand*. Ph.D. thesis, University of Wales, 147 pp.

Duller, G. A. T. 2005: *Luminescence Analyst*. 43 pp. University of Wales, Aberystwyth.

Durcan, J. A., Roberts, H. M., Duller, G. A. T. & Alizai, A. H. 2009: Testing the use of range-finder OSL dating to inform field sampling and laboratory processing strategies. *Quaternary Geochronology 5*, 86–90.

Galbraith, R. F. & Laslett, G. 1993: Statistical models for mixed fission track ages. *Radiation Measurements 21*, 459–470.
Gemmell, A. M. D. 1997: Fluctuations in the thermoluminescence signal of suspended sediemnt in an alpine glacial meltwater stream. *Quaternary Science Reviews 16*, 281–290.
Gemmell, A. M. D. 1999: IRSL from fine-grained glacifluvial sediment. *Quaternary Science Reviews 18*, 207–215.
Holtedahl, O. 1960: *Geology of Norway*. 540 pp. I Kommisjon Hos H. Aschehoug & Co., Oslo.
Holtedahl, O. & Dons, J. A. 1960: Geologisk kart over Norge Berggrunnskart (Geological map of Norway (Bedrock)). Scale 1: 1 000 000. *Norges Geologiske Undersøkelse 208*.
Huntley, D. J. & Baril, M. R. 1997: The K content of the K-feldspars being measured in optical dating or in thermoluminescence dating. *Ancient TL 15*, 11–13.
Huot, S. & Lamothe, M. 2003: Variability of infrared stimulated luminescence properties from fractured feldspar grains. *Radiation Measurements 37*, 499–503.
Jerlov, N. G. 1976: *Marine Optics*. 231 pp. Elsevier, New York.
King, G. E. 2012: *Fundamental and sedimentological controls on the luminescence of quartz and feldspar*. Ph.D. thesis, University of St Andrews, 372 pp.
King, G. E., Robinson, R. A. J. & Finch, A. A. 2013: Apparent OSL ages of modern deposits from Fåbergstølsdalen, Norway: implications for sampling glacial sediments. *Journal of Quaternary Science 28*, 673–682.
King, G. E., Robinson, R. A. J. & Finch, A. A. 2014: Towards successful OSL sampling strategies in glacial environments: deciphering the residual OSL signals of quartz and K-feldspar from modern glacial sediments. *Quaternary Science Reviews 89*, 94–107.
Kinnaird, T. C., Sanderson, D. C. W. & Woodward, N. L. 2012: Applying luminescence methods to geoarchaeology: a case study from Stronsay, Orkney. *Earth and Environmental Science Transactions of the Royal Society of Edinburgh 102*, 1–9.
Klasen, N., Fiebig, M., Preusser, F., Reitner, J. M. & Radtke, U. 2007: Luminescence dating of proglacial sediments from the Eastern Alps. *Quaternary International 164–165*, 21–32.
Lukas, S., Spencer, J. Q. G., Robinson, R. A. J. & Benn, D. I. 2007: Problems associated with luminescence dating of Late Quaternary glacial sediments in the NW Scottish Highlands. *Quaternary Geochronology 2*, 243–248.
Matthews, J. A., Olaf Dahl, S., Nesje, A., Berrisford, M. S. & Andersson, C. 2000: Holocene glacier variations in central Jotunheimen, southern Norway based on distal glaciolacustrine sediment cores. *Quaternary Science Reviews 19*, 1625–1647.
Mejdahl, V. 1979: Thermoluminescence dating: beta-dose attenuation in quartz grains. *Archaeometry 21*, 61–72.
Muñoz-Salinas, E., Bishop, P., Zamorano, J.-J. & Sanderson, D. 2012: Sedimentological processes in lahars: insights from optically stimulated luminescence analysis. *Geomorphology 136*, 106–113.
Munyikwa, K., Brown, S. & Kitabwalla, Z. 2012: Delineating stratigraphic breaks at the bases of postglacial eolian dunes in central Alberta, Canada using a portable OSL reader. *Earth Surface Processes and Landforms 37*, 1603–1614.
Murray, A. S. & Wintle, A. G. 2000: Luminescence dating of quartz using an improved single-aliquot regenerative-dose protocol. *Radiation Measurements 32*, 57–73.
Murray, A. S. & Wintle, A. G. 2003: The single aliquot regenerative dose protocol: potential for improvements in reliability. *Radiation Measurements 37*, 377–381.
Murray, A. S., Olley, J. M. & Caitcheon, G. G. 1995: Measurement of equivalent doses in quartz from contemporary water-lain sediments using optically stimulated luminescence. *Quaternary Science Reviews 14*, 365–371.
Nesje, A. & Kvamme, M. 1991: Holocene glacier and climate variations in western Norway: evidence for early Holocene glacier demise and multiple Neoglacial events. *Geology 19*, 610–612.
Nesje, A., Matthews, J. A., Dahl, S. O., Berrisford, M. S. & Andersson, C. 2001: Holocene glacier fluctuations of Flatebreen and winter-precipitation changes in the Jostedalsbreen region, western Norvay, based on glaciolacustrine sediment records. *The Holocene 11*, 267–280.
Nesje, A., Dahl, S. O., Andersson, C. & Matthews, J. A. 2000: The lacustrine sedimentary sequence in Sygneskardvatnet, western Norway: a continuous, high-resolution record of the Jostedalsbreen ice cap during the Holocene. *Quaternary Science Reviews 19*, 1047–1065.
R Development Core Team 2011: *R: A Language and Environment for Statistical Computing*. R Foundation for Statistical Computing, Vienna.
Readhead, M. L. 2002a: Absorbed dose fraction for ^{87}Rb β particles. *Ancient TL 20*, 25–28.
Readhead, M. L. 2002b: Addendum to 'Absorbed dose fraction for ^{87}Rb β particles'. *Ancient TL 20*, 47.
Rhodes, E. J. 2011: Optically stimulated luminescence dating of sediments over the past 200,000 years. *Annual Review of Earth and Planetary Sciences 39*, 461–488.
Rhodes, E. J. & Bailey, R. M. 1997: The effect of thermal transfer on the zeroing of the luminescence of quartz from recent glaciofluvial sediments. *Quaternary Science Reviews 16*, 291–298.
Rhodes, E. J. & Pownall, L. 1994: Zeroing of the OSL signal in quartz from young glaciofluvial sediments. *Radiation Measurements 23*, 581–585.
Rice, S. P. & Church, M. 2010: Grain-size sorting within rivers bars in relation to downstream fining along a wandering channel. *Sedimentology 57*, 232–251.
Roberts, H. M. 2007: Assessing the effectiveness of the double-SAR protocol in isolating a luminescence signal dominated by quartz. *Radiation Measurements 42*, 1627–1636.
Roberts, H. M. & Duller, G. A. T. 2004: Standardised growth curves for optical dating of sediment using multiple-grain aliquots. *Radiation Measurements 38*, 241–252.
Roberts, H. M., Durcan, J. A. & Duller, G. A. T. 2009: Exploring procedures for the rapid assessment of optically stimulated luminescence range-finder ages. *Radiation Measurements 44*, 582–587.
Sanderson, D. C. W. & Murphy, S. 2010: Using simple portable OSL measurements and laboratory characterisation to help understand complex and heterogeneous sediment sequences for luminescence dating. *Quaternary Geochronology 5*, 299–305.
Sanderson, D. C. W., Bishop, P., Houston, I. & Boonsener, M. 2001: Luminescence characterisation of quartz-rich cover sands from NE Thailand. *Quaternary Science Reviews 20*, 893–900.
Sanderson, D. C. W., Bishop, P., Stark, M. T. & Spencer, J. Q. 2003: Luminescence dating of anthropogenically reset canal sediments from Angkor Borei, Mekong Delta, Cambodia. *Quaternary Science Reviews 22*, 1111–1121.
Shakesby, R. A., Matthews, J. A. & Winkler, S. 2004: Glacier variations in Breheimen, southern Norway: relative-age dating of Holocene moraine complexes at six high-altitude glaciers. *The Holocene 14*, 899–910.
Stang, D. M., Rhodes, E. J. & Heimsath, A. M. 2012: Assessing soil mixing processes and rates using a portable OSL-IRSL reader: preliminary determinations. *Quaternary Geochronology 10*, 314–319.
Thiel, C. 2011: *On the applicability of post-IR IRSL dating to different environments*. Ph.D. thesis, Freien Universitat Berlin, 186 pp.
Thomsen, K. J., Murray, A. S., Jain, M. & Bøtter-Jensen, L. 2008: Laboratory fading rates of various luminescence signals from feldspar-rich sediment extracts. *Radiation Measurements 43*, 1474–1486.
Thrasher, I. M., Mauz, B., Chiverrell, R. C. & Lang, A. 2009: Luminescence dating of glaciofluvial deposits: a review. *Earth-Science Reviews 97*, 145–158.
Wallinga, J., Bos, A. J. J., Dorenbos, P., Murray, A. S. & Schokker, J. 2007: A test case for anomalous fading correction in IRSL dating. *Quaternary Geochronology 2*, 216–221.
Wallinga, J., Murray, A. & Wintle, A. 2000: The single-aliquot regenerative-dose (SAR) protocol applied to coarse-grain feldspar. *Radiation Measurements 32*, 529–533.
Wintle, A. G. 1973: Anomalous fading of thermoluminescence in mineral samples. *Nature 245*, 143–144.
Wintle, A. G. 2008: Luminescence dating: where it has been and where it is going. *Boreas 37*, 471–482.